# Core Loss Estimation in Electric Machines With Flux-Controlled Core Loss Tester

Burak Tekgun, *Member, IEEE*, Yilmaz Sozer, *Senior Member, IEEE*, Igor Tsukerman, Parag Upadhyay, *Senior Member, IEEE*, and Steven Englebretson

***Abstract*—The complexity of core loss estimation is a serious challenge in the design of high-efficiency electric machines. Current estimation methods based on the Steinmetz equation and loss separation are not accurate enough, even at the rated conditions. This paper describes a loss estimation technique combining finite-element analysis (FEA) and actual core loss measurements. First, flux density waveforms in various parts of the electric machine are determined using FEA. Second, the same waveforms are generated in a wound toroidal core made of the same material as used in the machine. The loss is measured per unit mass, and then the total motor core loss is calculated by integrating the measured W/kg loss values for predefined sections of the motor. These estimation results are compared with those of the Bertotti method. The proposed procedure is shown to improve the accuracy of loss estimation.**

***Index Terms*—Core loss estimation, core loss tester, flux controller.**

## I. Introduction

ENERGY efficiency has become one of the main concerns worldwide due to the rapid growth of global energy demand. Since electric machines dominate energy consumption, efficiency improvement of the machines has attracted significant interest for the past few decades. Over the years, electric machine efficiencies have been enhanced in parallel with the design techniques; many research groups have worked on the loss segregation of electrical machines [1]–[5]. In the past decade, the increasing popularity of electric vehicles, as well as more stringent government regulations concerning electric machine efficiencies [4], have further intensified the research in this area. Several methods have been developed to improve the efficiency and reduce the losses, especially for the electromagnetic iron losses as a dominant contribution. Although core losses in electrical machines have been investigated for more than a hundred years, core loss estimations are still lacking accuracy. The complexity of the dynamic nature of these losses and the measurement limitations make the analysis difficult. Moreover, it is challenging to determine the core losses associated with the magnetic field distortion, rotor ac fields, and rotating magnetic fields [6]. These losses are often lumped together into "stray load loss," which is not calculated but simply assumed as a percentage of the motor output power. The stray load losses may add up to 2% of the total output power in some cases [6]. The analysis, prediction, and consequent reduction of the mentioned losses are extremely important for designing high-efficiency electric machines.

There is a wide range of core loss estimation methods for electric machines—in particular, the Steinmetz equation, loss separation, and mathematical hysteresis models [7]. These models are designed for various purposes and differ from each other in some respects.

The origin of core loss modeling can be traced back to the landmark research of Steinmetz in 1892 [8]. Steinmetz modeled the core loss as an exponential function of frequency and of the peak flux density under sinusoidal excitation, in a limited range of frequencies and flux densities. Various approaches are developed to overcome these limitations and estimate losses for arbitrary waveforms, e.g., the modified Steinmetz equation (MSE) [9], the generalized Steinmetz equation (GSE) [10], improved GSE (iGSE) [11], and the natural Steinmetz equation (NSE) [12]. In another extension of the Steinmetz approach, known as loss separation or Bertotti method [7], the core loss is split into hysteresis, eddy current, excess loss, rotational loss, etc. Rotational losses, in particular, attracted significant attention [13].

Flux densities in motor yokes and transformer T-joints may be nonsinusoidal and sometimes contain dc components. Similarly to the previously presented loss separation methods, rotational losses are considered as another dynamic loss component [14]–[17]. In this model, rotational losses, higher order harmonic losses, and linear magnetizing losses are combined to calculate the core losses [7]. In another approximation [18], a correction factor is introduced to incorporate rotational losses into the Bertotti model. Another focus in loss separation models

Manuscript received September 9, 2017; revised February 14, 2018 and May 18, 2018; accepted July 13, 2018. Date of publication October 8, 2018; date of current version February 20, 2019. Paper 2017-EMC-0664.R2, presented at the 2016 IEEE Energy Conversion Congress and Exposition (ECCE), Milwaukee, WI, USA, September 18–22, approved for publication in the IEEE Transactions on Industry Applications by the Electric Machines Committee of the IEEE Industry Application Society. This work was supported by fellowships from ABB US Corporate Research. The work of I. Tsukerman was supported in part by the U.S. National Science Foundation under Grant DMS-1620112. *(Corresponding author: Yilmaz Sozer.)*

B. Tekgun was with the Department of Electrical and Computer Engineering, The University of Akron, Akron, OH 44325 USA. He is now with the Department of Electrical Electronics Engineering, Abdullah Gul University, Kayseri 38080, Turkey (e-mail: burak.tekgun@agu.edu.tr).

Y. Sozer and I. Tsukerman are with the Department of Electrical and Computer Engineering, The University of Akron, Akron, OH 44325 USA (e-mail: ys@uakron.edu; igor@uakron.edu).

P. Upadhyay and S. Englebretson are with the ABB US Corporate Research Center, Raleigh, NC 27606 USA (e-mail: parag.upadhyay@us.abb.com; steven.englebretson@us.abb.com).

Color versions of one or more of the figures in this paper are available online at http://ieeexplore.ieee.org.

Digital Object Identifier 10.1109/TIA.2018.2874352

is the influence of high-frequency pulsewidth-modulated (PWM) excitation [19], [20]. In one major study [5], core losses of a PWM voltage-fed machine are separated into hysteresis, Eddy current based on average rectified, and rms values of the PWM voltage.

The Steinmetz equation and loss separation models are engineering-oriented and partly heuristic approaches. More accurate models use material properties and hysteresis curves to represent the physical phenomena behind the electromagnetic losses. For hysteresis, in particular, the Preisach [21] and Jilles-Atherton models [22], [23] are the most notable ones, with various amendments [24]–[26]. These physical models are applicable to arbitrary waveforms, dc offset, and minor hysteresis loops.

Due to their practical, straightforward structures, Steinmetz equation and the loss separation models are popular and useful for rough core loss estimation, e.g., in finite-element analysis (FEA) software [10]. However, the estimation error varies depending on the application. In some cases, this error exceeds 100%, especially in electric machines where higher-order harmonics and dc-biased waveforms are present. Mathematical hysteresis models can be more accurate than the Steinmetz-equation- and loss-separation-based models but are complex and require much more knowledge about the material and testing. Integration of hysteresis loss models into FEA may be difficult or not even possible, and the simulations are time-consuming [26].

The core loss measurement is as important as the core loss estimation, and a variety of methods have been used [27], [28]. The four-wire technique [14] has been used in many applications requiring high accuracy measurements [6], [29]. This method employs a toroidal transformer with two or more windings on a test core. A primary winding is used for excitation, while other windings are used for sensing the induced voltage. The core loss can be calculated by integration of the product of the sensed voltage and the current passing through the primary winding. The method provides very fast and accurate *BH* loop determination through the sense coil voltage and the primary winding current [30]. However, it is quite sensitive to the phase discrepancy. Due to the physical limitations of the current measurement devices, current waveforms are captured with a certain delay, which results in errors [6]. To avoid this problem, precision resistors can be used instead of Hall Effect current transducers. Otherwise, measured current data should be corrected by introducing a phase advance if the current transducer's propagation delay is constant for a wide range of frequencies. Another important aspect that influences the core losses is temperature variation [6]. Hence, the measurement process should be kept as fast as possible with an automated system to avoid the temperature variation.

We propose a novel core loss estimation technique that combines FEA with core loss measurements. The method begins with an FEA of the electric machine. Flux waveforms are obtained in different regions where the loss is approximately uniform. Then the same flux density waveforms are generated in a toroidal wound core made of the same material as is used in the machine, with a novel flux-controlled core loss tester unit shown in Fig. 1.

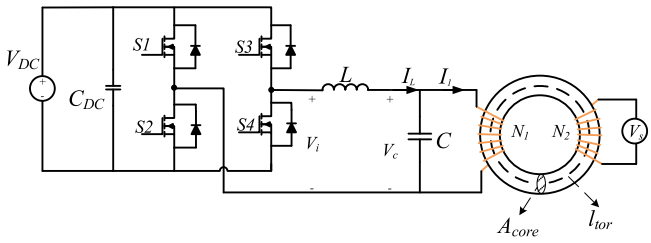


Fig. 1. Flux-controlled core loss tester.

The core loss tester is capable of controlling both dc and ac flux densities. The core loss is measured per unit mass of the material. This allows actual core loss measurements under known and controllable flux density waveforms. Finally, the corresponding core loss per mass/volume data for the different regions and flux density waveforms are combined to calculate the total core loss in the motor.

It should be noted that only unidirectional flux densities are considered in this paper, similarly to the magnetic circuit loss models [31], [32]. There are custom test setups in the literature for measuring the rotational losses, but the toroidal tester allows the core loss test only in one direction. It is possible to estimate rotational losses using superposition of alternating losses. Results may be reasonable for some materials at low flux density levels. However, the superposition method overestimates the losses when the material is saturated [33]. Considering that the percentage of the stator core volume subjected to the rotational losses is varying between 15% and 30% depending on the machine size (from 1 kW to 44.8 MW), and the relevant core loss increase varies between 2% and 28% [34], [35], the effect of the rotational losses is not significant for the target $<$10% error threshold for small- and medium-sized machines.

As a practical engineering approach, this method answers the question of how a particular core material would behave under certain flux density conditions. Consequently, the loss estimation becomes more realistic and accurate.

The following section gives further details about the proposed core loss estimation method. The flux-controlled core loss tester, core loss measurements and the aspects affecting the accuracy are explained in Section III. In Section IV, a case study is presented for a 10-hp interior permanent-magnet synchronous motor (IPMSM). The results of the proposed core loss estimation method are compared with those of the Bertotti core loss estimation method.

## II. Core Loss Estimation Method

The model is a combination of FEA and core loss measurements. The estimation procedure is given in Fig. 2. The method begins with an FEA of the electric machine. Then, the flux density waveforms are obtained from different regions where the loss is approximately uniform. The third step is to generate the same flux density waveforms in a test core made out of the same material as is used in the machine and to analyze the core losses under these waveforms. This requires a signal generator and a toroidal core loss tester. Instead of the

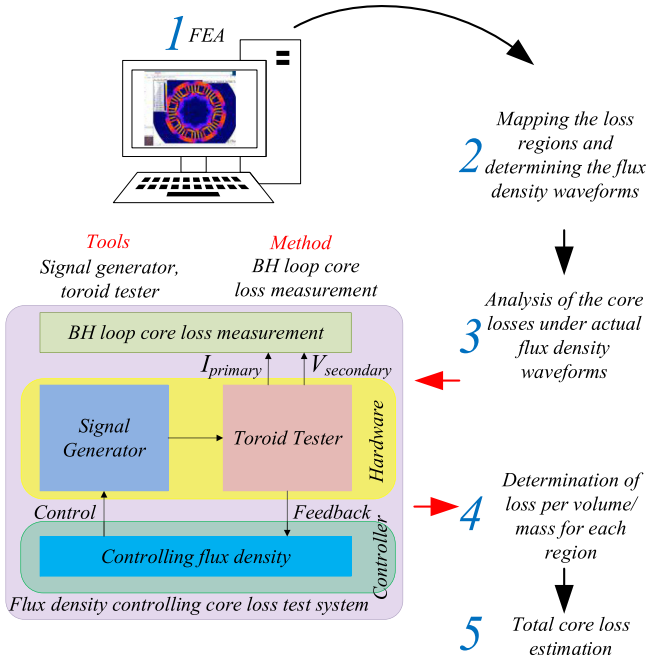


Fig. 2. Proposed core loss estimation procedure.

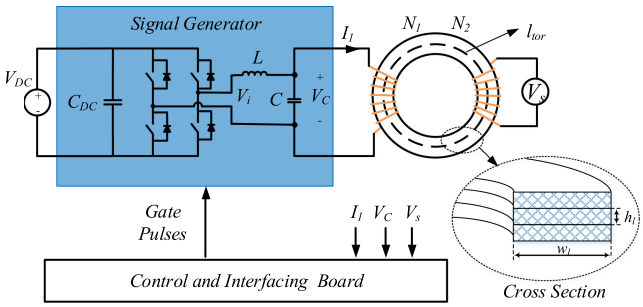


Fig. 3. Proposed core loss test system.

conventional voltage controlled signal generator, we use a flux controlling signal generator that we developed earlier [36]. The core loss tester must be able to control the ac and dc flux densities in the core under test (CUT), so that the obtained flux density waveforms from the rotor and stator are generated accurately. Next, the core losses are measured with the *BH* loop method and associated with the mass/volume of the material for each region. The final step is to estimate the total core loss of the motor by combining the loss per mass/volume data for each region from the toroidal core measurements.

## III. Flux-Controlled Core Loss Tester and Core Loss Measurements

In order to generate the desired flux density waveforms, hardware consisting of a high bandwidth signal generator and a toroid tester are needed. The proposed test system shown in Fig. 3 is designed for the *BH* loop core loss test. In this method, the dc input voltage is processed with the H-bridge inverter, and the signal at the desired frequency and shape is applied to the toroid transformer. Then, the flux density and field strength are calculated instantaneously from the measured quantities $V_s$ and $I_1$.

Two different toroidal transformers are built, one from the stator laminations and another one from the rotor laminations. The toroidal core sample dimensions are decided based on the available area on the stator and rotor laminations of the motor. To minimize further influence on the core losses, the widths of the core sample are kept as large as possible. Three ring-shaped laminations are cut out for each transformer from the actual motor laminations. The first toroid has 0.5 mm thickness $(h_l)$, 14 mm width $(w_l)$, and 57.2 cm core length $(l_{tor})$, and the second toroid has 0.675 mm thickness, 9 mm width, and 16 cm core length. It should be noted that the sample width of the first toroid is larger than the width of the stator teeth and smaller than the stator yoke thickness. This estimation process may be made more accurate by using two samples, one of them having the width of the stator teeth and the other one having the width equal to the stator yoke thickness because the magnetic properties of the samples having smaller widths differ from the samples having larger widths [37]. In this paper, only one sample that has 14 mm thickness is used for the stator core loss estimation.

Although the laminations are welded in the actual motor, the core samples are glued together to avoid width variations through the stacked sample. It is known that the magnetic properties of the material are affected by the manufacturing process [38], which influences the core loss significantly [39], [40]. Since the laminations used in this paper are taken from an actual motor, the material has already undergone the manufacturing processes. In addition, during the sample preparation process, the laminations are cut again, which degrades the magnetic properties, and glued together, which causes an axial stress on the sample, further affecting the core loss. Therefore, it can be assumed that the measured core loss from the toroidal tester would be slightly higher than it is in the motor.

The flux linkage $\lambda$ is calculated through the integration of the voltage measured from the sense coil; then the flux density $B$ can be calculated as

$$B = \frac{1}{N_2 A_{\text{core}}} \underbrace{\int V_s(t)\, dt}_{\lambda} \tag{1}$$

where $N_2$ is the number of turns on the sense coil, $A_{\text{core}}$ is the cross-sectional area of the core, and $V_s$ is the induced voltage on the sensing winding.

The developed core loss tester is presented in Fig. 4. It consists of an SiC single-phase H-bridge inverter operating at 150 kHz, an *LC* filter with 10 kHz bandwidth, and a toroidal inductor that has two windings on a core under test. A Texas Instruments floating point dual-core DSP microcontroller TMS320F28377D is used for control with a sampling time $T_s = 6.6\ \mu\text{s}$ $(f_s = 150\ \text{kHz})$. The control and interfacing unit can be seen in Fig. 4(c). The tester has a 130 A peak current, 900 V peak voltage, and a 10 kHz fundamental frequency limit.

The filter capacitor voltage, the inductor current, and the secondary winding voltage are fed back to the digital controller which controls the secondary winding voltage directly and the ac

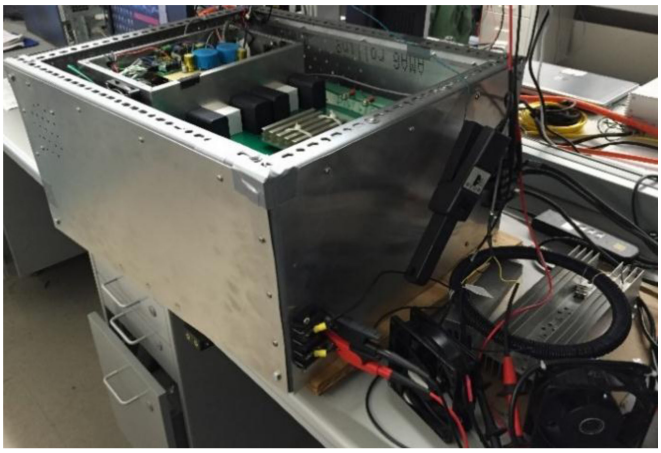

(a)

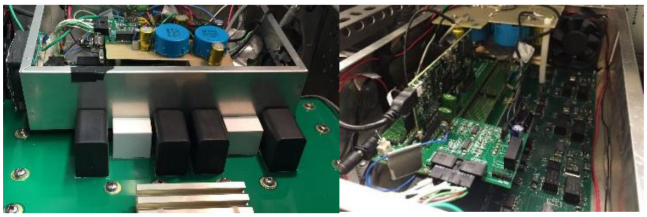

(b) (c)

Fig. 4. (a) Core loss tester. (b) Power circuitry and dc bus. (c) Control and interfacing unit.

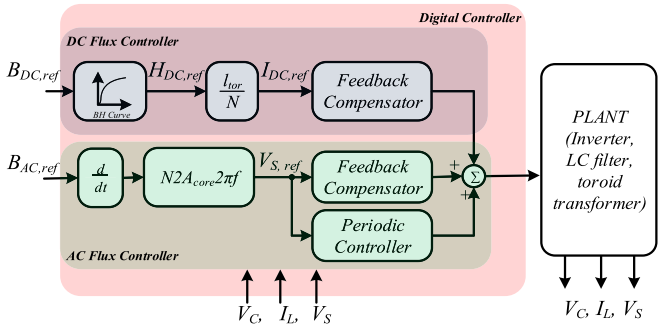


Fig. 5. Flux controller structure.

component of the flux indirectly. The digital controller shown in Fig. 5 uses repetitive control and state feedback control schemes to track the reference signal. The repetitive control suppresses the periodic disturbances and guarantees the zero steady-state error while the state feedback controller gets rid of nonperiodic disturbances. DC flux level is controlled by another feedback controller that uses the average filter inductor current. Thus, arbitrary flux density waveforms can be generated in the core at a wide range of frequencies with/without dc offset. The complete control structure is given in Fig. 5, the detailed system modeling and control design can be found in [36].

For a valid and accurate core loss measurement, it is important to have a proper understanding of various measurement errors. The measurement system may be affected by phase discrepancy between the measured voltage and current waveforms due to the poor frequency response of the current sensor, by the temperature of the core, etc. In order to mitigate the phase discrepancy,

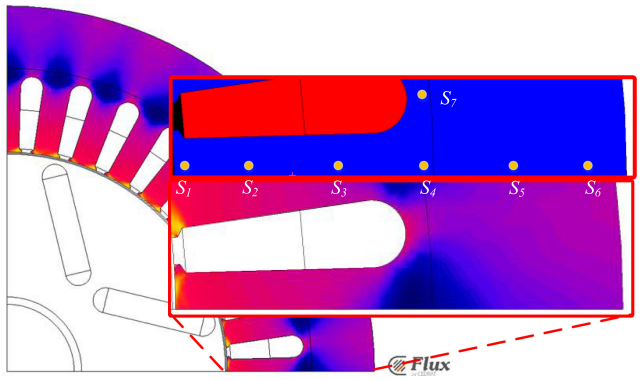


Fig. 6. Stator core loss distribution and the selected regions.

a precision (low inductance) resistor was used. The influence of temperature was minimized by keeping the measurement time short; therefore, temperature variations due to the high current levels are avoided.

## IV. Core Loss Estimation of an IPMSM

A 10-hp, four-pole, 36-slot, 1800-r/min IPM motor is selected to analyze for the proposed estimation method. First, the core loss regions are determined. Second, the flux density waveforms of these regions are recorded for no-load and loaded cases, and finally, these waveforms are generated on the toroidal core and core loss is measured to be used in the estimation.

### A. Determination of Loss Regions

The motor core loss regions are determined using FEA of the motor under rated conditions. The sampling ratio on the FEA simulation is 20 $\mu$s (50 kHz), which allows us to capture harmonics up to 25 kHz in the flux density waveforms. Given that the flux-controlled signal generator's bandwidth is 10 kHz [36], the captured waveforms have enough resolution to be rebuilt in the flux-controlled tester. Moreover, the motor is fed with sinusoidal currents in FEA and during the tests, so there is not PWM-related harmonic content in the waveforms under consideration. The cross-sectional core loss distribution in the motor was estimated using the conventional Bertotti model because it accounts for the flux density rate of change; hence, high-frequency effects can be distinguished easily. The estimated core loss using Bertotti's method is displayed in Fig. 6.

Determining the rotor core loss regions is a little different for the stator because the core loss per volume values differ from one region to another significantly. Therefore, distinguishing the regions from each other is not as easy as is the case in the stator. In order to visualize the loss distribution through the rotor, different color scales are used, as shown in Fig. 7(a), (b), and (c). The minimum limit is 0 W/kg, and the maximum limits are 124 000 W/m$^3$ for Fig. 7(a), 12 400 W/m$^3$ for Fig. 7(b), and 4100 W/m$^3$ for Fig. 7(c). The loss regions are determined, as shown in Fig. 7(d).

The estimation gets more accurate as the cross-sectional sectors of the motor get denser. This is conceptually similar to FEA simulations, where denser meshes can capture the local

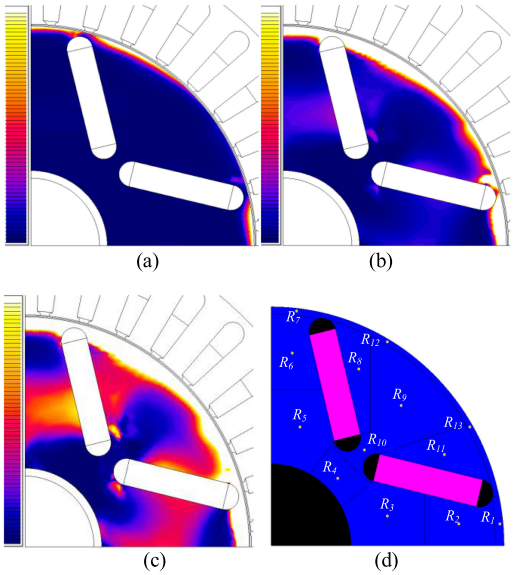


Fig. 7. Rotor loss distribution using different color scales. The maximum values of core loss per volume are (a) 124 000 W/m$^3$, (b) 12 400 W/m$^3$, and (c) 4100 W/m$^3$. (d) Rotor core loss regions.

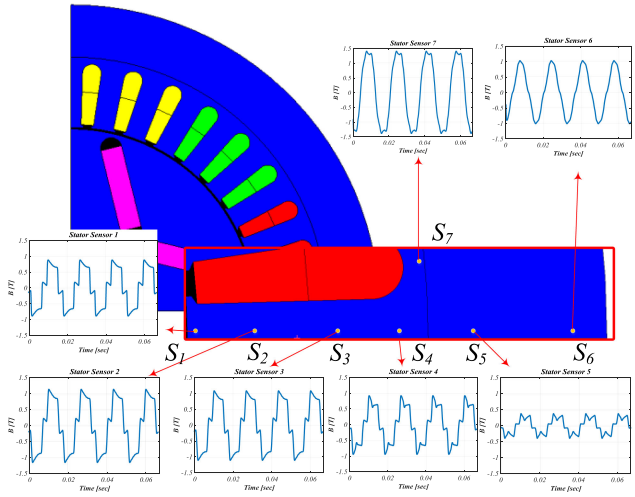


Fig. 8. Flux density waveforms of a stator of an IPMSM.

variations of flux densities and generate more accurate results. However, accurate core loss estimation can be achieved if the sectoring is done carefully, which will also shorten the estimation process [31], [41], [42].

### *B. Determination of Flux Density Waveforms of the IPMSM*

After determining the motor core loss regions, the flux density waveforms of the motor for the no-load conditions have been obtained from the FEA by placing flux sensors in the middle of each loss region. When the motor is not loaded, the averaged input power includes only the stator copper loss, the friction and windage loss, and the core loss. The copper loss can be calculated using the stator winding resistance and the current passing through them. It should be noted that the stator resistance varies with the temperature and the expression for the new resistance value is as follows:

$$R = R_0 \left(1 + \alpha_{\mathrm{Cu}} \left(T - T_0\right)\right) \tag{2}$$

where $R_0$ is the measured ac resistance at 25 °C, $\alpha_{\mathrm{Cu}}$ $(0.004041)$ is the temperature coefficient of copper, and $T_0$ is the reference temperature which is 25 °C for our case. The winding temperature can be measured with the thermocouples placed between the windings. Before taking any further measurements, the motor should be running for about 30 min at the rated load until the temperature of the windings is stabilized. Then, each measurement can be taken at the rated operation temperature. Therefore, the measurement error can be minimized. In this paper, all the measurements are performed at the rated operating temperature of 40 °C. Phase resistance at 25 °C is measured as 0.651 Ω and calculated as 0.6905 Ω for 40 °C. If there is ±2 °C temperature measurement error, the copper loss variation is ±0.75% for the rated loading condition (10 A rated current, 205.6 W at 38 °C, 208.7 W at 42 °C); ±0.76% for the no-load condition (7 A, 462 V, 100.72 W at 38 °C, 102.27 W at 42 °C). For the measured core loss of ∼125 W at no load, the stator copper loss measurement error (±0.775 W) does not have a significant effect on the core loss measurement accuracy, as long as the measurement temperature is kept constant.

Mechanical losses can be determined using the IEEE standard regarding the friction and windage loss determination section [43]. Although different samples of a machine manufactured at the same facility are assumed to have the same features, their performance and losses slightly vary from each other. Especially, the mechanical losses vary as the machine ages, collects dust, etc. In this paper, mechanical loss of the machine is considered constant at the rated speed and is measured at the manufacturing facility as 98 W, which is 1.3% of the rated power of the machine.

The core loss can be measured by performing the no-load test. For the no-load condition, the averaged input power should be equal to the summation of the copper, friction – windage, and core losses. This allows the input current to be calculated and applied to the FEA model of the motor. The resulting flux density waveforms are presented in Figs. 8 and 9. While the stator flux density waveforms are zero-mean ac signals with a 60 Hz fundamental and higher order harmonics, the rotor waveforms contain a 1080 Hz ac fundamental and higher order harmonics, in addition to a dc offset. The 1080 Hz fundamental frequency is the result of the stator teeth passing through the rotor poles. The dc offset varies in different regions depending on the flux path and the rotor geometry.

A closer look at the earlier waveforms reveals that the stator Sensor 1 ($S_1$) has a 60 Hz frequency fundamental. This waveform becomes distorted and additional high-frequency components are added to the 60 Hz waveform when the motor is loaded. Because the position of the sensor is close to the air gap, the waveform includes harmonics caused by the air gap flux, rotor slots, instantaneous field variations at the magnet ends, etc. On the stator Sensor 2 ($S_2$), the waveform amplitude increases due to the narrowing flux path, which increases the saturation of the core material. Similarly, this waveform also includes high-frequency harmonics when the motor is loaded. However, the

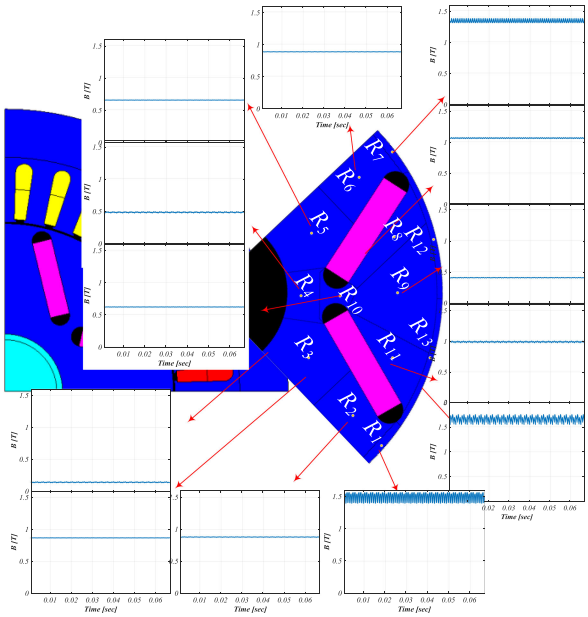


Fig. 9. Flux density waveforms of a rotor of an IPMSM.

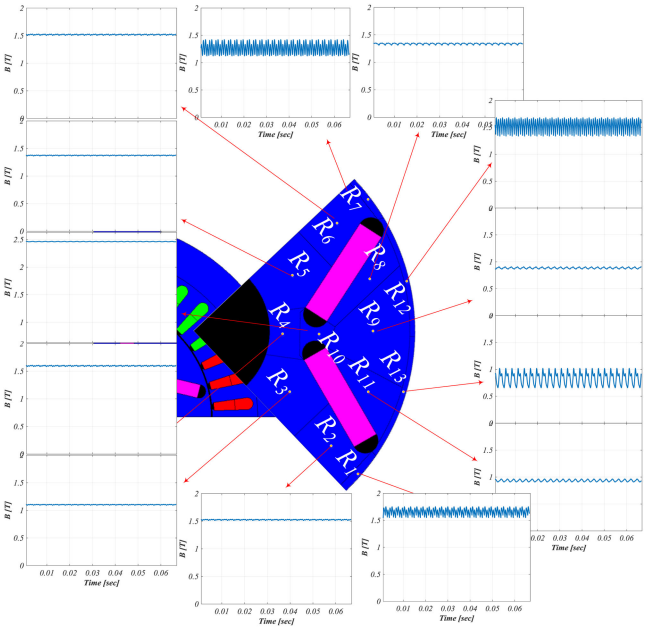


Fig. 11. Rotor flux density waveforms of an IPMSM at loaded conditions.

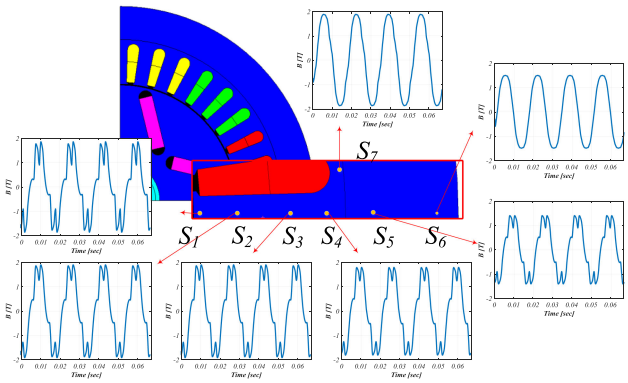


Fig. 10. Stator flux density waveforms of an IPMSM at loaded conditions.

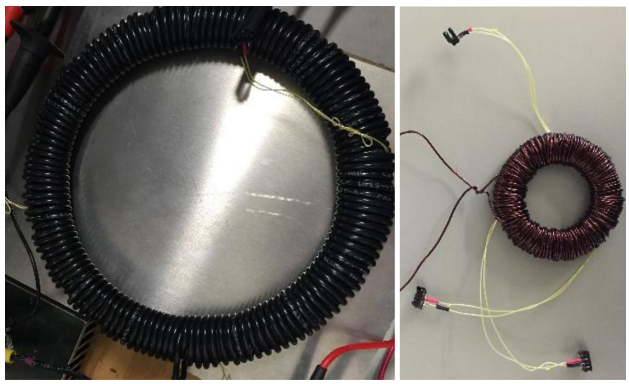

Fig. 12. Prepared toroid transformers for testing.

high-frequency component is not as significant as in the S1 sensor. The Sensor 3 ($S_3$) waveform has similar properties to those of $S_2$. Sensor 4 ($S_4$) measures similar output to those of Sensor 3 ($S_3$) having even lower high-frequency components. At the yoke of the motor, the flux density decreases because the flux path widens, as seen from Sensors 5 ($S_5$) and 6 ($S_6$).

The same procedure is followed for the determination of the flux density waveforms for the rated conditions. The current level is set to produce the rated torque and the waveforms are taken, as presented in Figs. 10 and 11.

It can be clearly seen from the figures that the amplitudes of the fundamental and harmonic components increase with load, which leads to a significant increase in the core losses.

### C. Core Loss Tests Under Actual Flux Density Waveforms

Once the waveforms are obtained, the proposed method requires generating the same flux waveforms in the core made of the same material as is used in the machine. Hence, two toroidal transformers have been wound on the stator and rotor electrical steels. To avoid measurement errors due to capacitive couplings and leakage inductances, the primary and secondary windings are placed on top of each other and wound as tightly as possible (see Fig. 12) [6].

The toroid made out of the stator material has 264 turns on the primary and 30 turns on the secondary windings. The measured magnetizing inductance is 2.21 mH, the leakage inductance is 200 $\mu$H, and the dc resistance is 330 m$\Omega$. The second toroid is made of the steel used in rotor laminations. To reach the desired dc offset for the magnetic field, the number of turns in the primary winding has been increased to 300 and the core size decreased. The sample has three individual secondary windings to adjust the secondary winding voltage amplitude. The magnetizing inductance, leakage inductance, and the dc resistance of the second toroid are 14.9 mH, 340 $\mu$H, and 2.11 $\Omega$, respectively.

The flux-controlled core loss tester is used to generate the flux density waveforms obtained from the FEA. For a given flux density waveform, the core loss tester generates the required voltage waveform on the secondary winding. Fig. 13

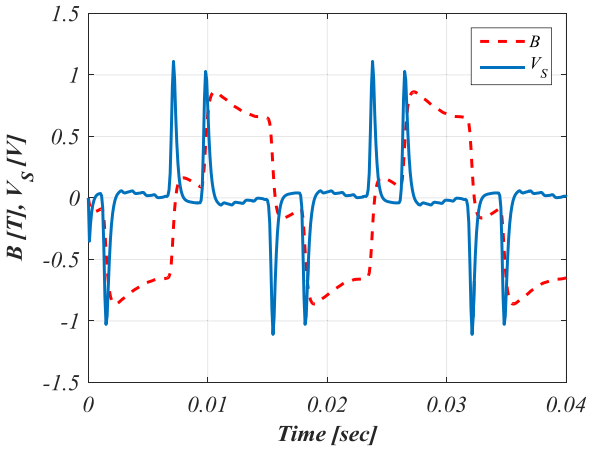


Fig. 13. Flux density waveform of the stator sensor $S_1$ and the corresponding secondary winding voltage.

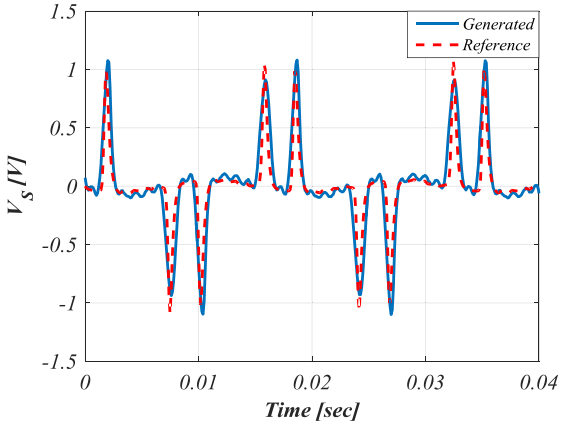


Fig. 14. Reference and generated secondary winding voltages.

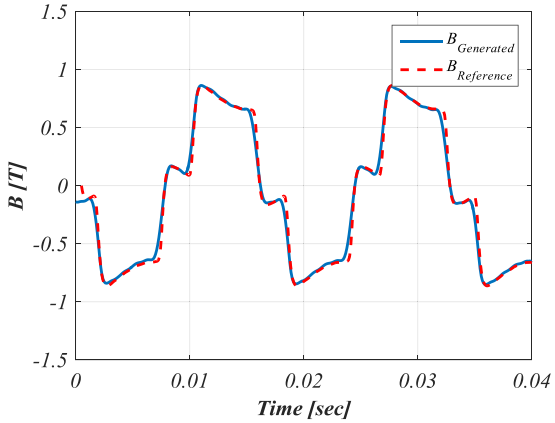


Fig. 15. Reference and generated flux density waveform of $S_1$.

shows the flux density and the corresponding secondary voltage waveforms.

Figs. 14 and 15 present the reference and generated waveforms of the secondary winding voltage and the flux density waveforms for the stator sensor $S_1$.

Similarly, other flux density waveforms from the regions given in Fig. 8 are generated. The sensors $R_{12}$ waveform is given in Fig. 16 as an example.

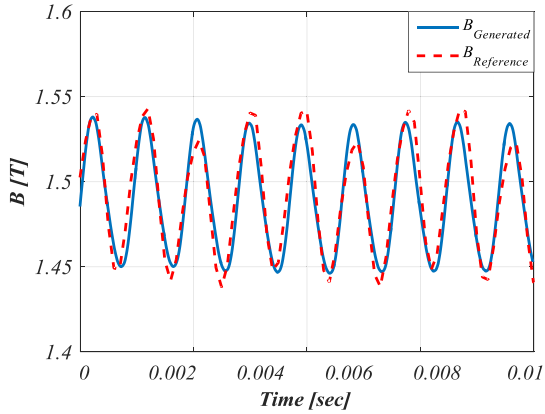


Fig. 16. Flux density waveform of the motor from the rotor sensor $R_{12}$.

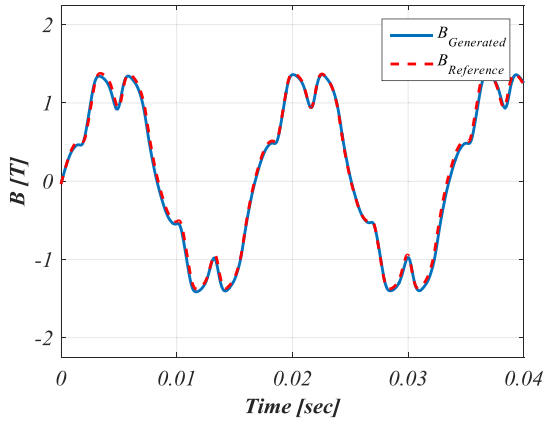


Fig. 17. Reference and generated flux density waveform of $S_5$ at the rated loading condition.

The rotor flux density waveforms in Fig. 9 contain a dc offset and high-frequency components. Because these waveforms are taken at the no-load conditions, the high-frequency components are not very significant except for some of the regions. These high-frequency components grow when the motor is loaded, which causes the rotor core loss to increase rapidly. Fig. 16 shows the flux density waveform of the motor taken from the rotor sensor $R_{12}$, which exhibits the largest high-frequency oscillation. The waveform taken from the same region at the rated conditions has a dc offset exceeding 1.5 T, with a high-frequency component of 0.1 T in peak-to-peak amplitude.

The waveforms obtained from the FEA at the rated loading conditions are generated in the test system as well. Fig. 17 presents the reference and generated flux density waveform for the fifth stator core loss region.

Again, the rotor waveforms contain different levels of dc offsets and high-frequency components that have higher amplitudes than the ones in no-load condition. Figs. 18 and 19 show the reference and generated flux density waveforms of the fourth and twelfth rotor core loss regions at the rated loading condition.

The power loss is measured when the waveforms are generated for each region. Verification of the core loss measurement is done with an energy analyzer by feeding the primary winding

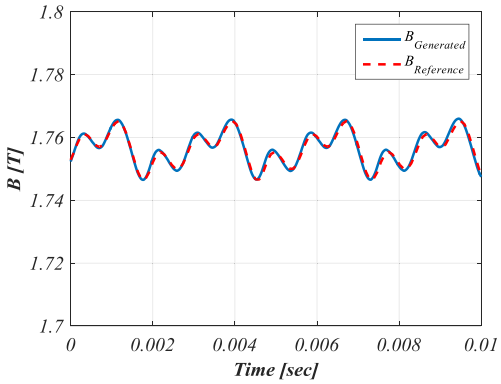


Fig. 18. Reference and generated flux density waveform of $R_4$ at the rated loading condition.

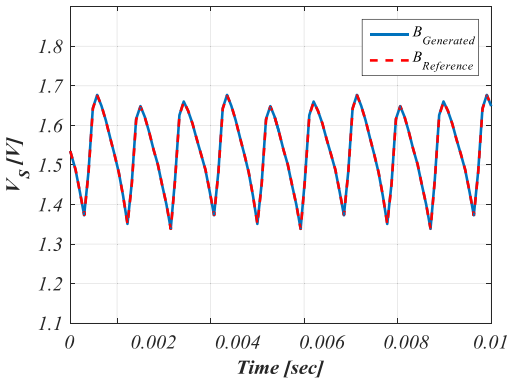


Fig. 19. Reference and generated flux density waveform of $R_{12}$ at the rated loading condition.

TABLE I
CORE LOSS PER MASS DATA FOR EACH STATOR LOSS REGION AT THE NO-LOAD CONDITION

| *Loss Region* | *Core loss [W/kg]* | *Mass of the region [kg]* |
|---|---|---|
| *1* | *9.5* | *0.5361* |
| *2* | *10.4* | *1.0722* |
| *3* | *10.4* | *1.0722* |
| *4* | *7.4* | *1.0186* |
| *5* | *4.3* | *1.1901* |
| *6* | *7.6* | *8.6874* |
| *7* | *9.4* | *1.0293* |
| *Total stator core loss* | | *115.5 W* |

current and the sense coil voltages to the device. The core loss per mass data for the stator and rotor loss regions, along with the mass of each region, are given in Tables I and II for no-load conditions.

The estimated total stator core loss is 115.5 W. Similarly, total no-load rotor core loss is calculated as 6 W by adding up the losses of the rotor regions. Hence, the total no-load core loss is estimated at 121.5 W, which is very close to the measured value of 125 W using the *IEEE* motor loss segregation standard.

TABLE II
CORE LOSS PER MASS DATA FOR EACH ROTOR LOSS REGION AT THE NO-LOAD CONDITION

| *Loss Region* | *Core loss [W/kg]* | *Mass of the region [kg]* |
|---|---|---|
| *1* | *3.11* | *0.53* |
| *2* | *0.65* | *0.55* |
| *3* | *0.41* | *0.81* |
| *4* | *0.35* | *1.10* |
| *5* | *0.92* | *1.26* |
| *6* | *0.74* | *0.38* |
| *7* | *1.85* | *0.40* |
| *8* | *0.66* | *0.65* |
| *9* | *0.52* | *1.02* |
| *10* | *1.58* | *1.11* |
| *11* | *1.22* | *0.71* |
| *12* | *3.15* | *0.68* |
| *13* | *3.44* | *0.49* |
| *Total stator core loss* | | *6 W* |

TABLE III
CORE LOSS PER MASS DATA FOR EACH STATOR LOSS REGION AT THE RATED LOADING CONDITION

| *Loss Region* | *Core loss [W/kg]* | *Mass of the region [kg]* |
|---|---|---|
| *1* | *15.6* | *0.5361* |
| *2* | *14.6* | *1.0722* |
| *3* | *14.6* | *1.0722* |
| *4* | *9* | *1.0186* |
| *5* | *5.2* | *1.1901* |
| *6* | *8.1* | *8.6874* |
| *7* | *10.1* | *1.0293* |
| *Total stator core loss* | | *135.5 W* |

Using the proposed method, the total core loss of the motor is estimated accurately when the motor is not loaded (classical iron losses). The results are compared with those of the method used in the Flux 2D FEA software package; that is, Bertotti's core loss model, in which the total core loss is calculated as 67 W.

Using the measured loss for the flux density waveforms given in Figs. 10 and 11, Tables III and IV are created. The estimated total core loss is 150 W, which includes a 135.5 W loss in the stator and a 14.5 W loss in the rotor.

The Bertotti loss model results in total losses of 106 W at the loaded condition, in contrast with the proposed model, which gives 150 W. At present, there is no standard method for measuring the core losses at the rated conditions to verify the accuracy of the proposed method.

TABLE IV
CORE LOSS PER MASS DATA FOR EACH ROTOR LOSS REGION AT THE RATED LOADING CONDITION

| *Loss Region* | *Core loss [W/kg]* | *Mass of the region [kg]* |
|---|---|---|
| *1* | *9* | *0.53* |
| *2* | *1.2* | *0.55* |
| *3* | *1.23* | *0.81* |
| *4* | *4.35* | *1.10* |
| *5* | *1.95* | *1.26* |
| *6* | *0.795* | *0.38* |
| *7* | *7.5* | *0.40* |
| *8* | *1.8* | *0.65* |
| *9* | *1.05* | *1.02* |
| *10* | *9.6* | *1.11* |
| *11* | *1.65* | *0.71* |
| *12* | *6.3* | *0.68* |
| *13* | *4.5* | *0.49* |
| *Total stator core loss* | | *14.5 W* |

## V. CONCLUSION

The proposed core loss estimation method for electric machines employs a flux-controlled core loss test unit. This unit is capable of controlling ac and dc flux densities in a toroidal core, to mimic the actual flux waveforms in various parts of electric machines. These flux waveforms are determined from FEA and generated in the core during the test. The resulting core loss values for the applied flux density waveforms are captured and prorated, on a per-unit-mass basis, to the total loss in the motor.

The proposed method is applied to an interior permanent-magnet synchronous motor at no-load conditions and compared with the experimental measurements. The results show that the proposed method provides very accurate estimates of the core loss under no-load conditions. Verification of the method under the loaded condition is an integral part of our future work.

## ACKNOWLEDGMENT

The authors would like to thank Dr. Rich Schiferl, Dr. Stephen D. Umans, and Dr. Boris Shoykhet for their valuable comments and suggestions.

## REFERENCES

[1] D. L. Atherton and D. C. Jiles, "Effects of stress on magnetisation of steel," *IEEE Trans. Magn.*, vol. 19, no. 5, p. 2021, Sep. 1983.
[2] E. Dlala, A. Belahcen, J. Pippuri, and A. Arkkio, "Interdependence of hysteresis and eddy-current losses in laminated magnetic cores of electrical machines," *IEEE Trans. Magn.*, vol. 46, no. 2, pp. 306–309, Feb. 2010.
[3] A. Krings, S. A. Mousavi, O. Wallmark, and J. Soulard, "Temperature influence of NiFe steel laminations on the characteristics of small slotless permanent magnet machines," *IEEE Trans. Magn.*, vol. 49, no. 7, pp. 4064–4067, Jul. 2013.
[4] B. Tekgun, Y. Sozer, and I. Tsukerman, "Modeling and parameter estimation of split-single phase induction motors," *IEEE Trans. Ind. Appl.*, vol. 52, no. 2, pp. 1431–1440, Mar.-Apr. 2016.
[5] A. Boglietti, A. Cavagnino, D. M. Ionel, M. Popescu, D. A. Staton, and S. Vaschetto, "A general model to predict the iron losses in PWM inverter-fed induction motors," *IEEE Trans. Ind. Appl.*, vol. 46, no. 5, pp. 1882–1890, Sep. 2010.
[6] B. Tekgun, Y. Sozer, and I. Tsukerman, "Measurement of core losses in electrical steel in the saturation region under DC bias conditions," *IEEE Trans. Ind. Appl.*, vol. 53, no. 1, pp. 88–96, Jan. 2017.
[7] A. Krings and J. Soulard, "Overview and comparison of iron loss models for electrical machines," *J. Electr. Eng.*, vol. 10, pp. 162–169, 2010.
[8] C. P. Steinmetz, "On the law of hysteresis," *J. Exp. Anal. Behav.*, vol. 13, no. 2, pp. 243–266, 1984.
[9] J. Reinert, A. Brockmeyer, and R. W. A. A. De Doncker, "Calculation of losses in ferro- and ferri-magnetic materials based on the modified Steinmetz equation," *IEEE Trans. Ind. Appl.*, vol. 37, no. 4, pp. 1055–1061, Jul./Aug. 2001.
[10] J. L. J. Li, T. Abdallah, and C. R. Sullivan, "Improved calculation of core loss with nonsinusoidal waveforms," in *Proc. IEEE Ind. Appl. Conf.*, 2001, vol. 4, no. C, pp. 2203–2210.
[11] K. Venkatachalam, C. R. Sullivan, T. Abdallah, and H. Tacca, "Accurate prediction of ferrite core loss with nonsinusoidal waveforms using only Steinmetz parameters," in *Proc. IEEE Workshop Comp. Power Electron.*, 2002, no. Jun. pp. 36–41.
[12] A. van Den Bossche, V. C. Valchev, and G. B. Georgiev, "Measurement and loss model of ferrites with non-sinusoidal waveforms," in *Proc. PESC Rec. IEEE Annu. Power Electron. Spec. Conf.*, 2004, vol. 6, no. 1, pp. 4814–4818.
[13] V. Pricop, "Hysteresis effects in the cores of particle accelerator magnets," Transylvania Univ., Brasov, Romania, 2016.
[14] A. Krings and J. Soulard, "Overview and comparison of iron loss models for electrical machines," *J. Electr. Eng.*, vol. 10, no. 3, pp. 162–169, 2010.
[15] W. A. Pluta, "Some properties of factors of specific total loss components in electrical steel," *IEEE Trans. Magn.*, vol. 46, no. 2, pp. 322–325, Feb. 2010.
[16] K. Atallah and D. Howe, "Calculation of the rotational power loss electrical steel laminations from measured H and B," *IEEE Trans. Magn.*, vol. 29, no. 6 pt. 2, pp. 3547–3549, Nov. 1993.
[17] N. Alatawneh, S. Member, P. Pillay, S. Member, and P. Pillay, "Design of a novel test fixture to measure rotational core losses in machine laminations," *IEEE Trans. Ind. Appl.*, vol. 48, no. 5, pp. 1467–1477, Sep. 2012.
[18] S. Jacobs *et al.*, "Magnetic material optimization for hybrid vehicle PMSM drives," *World Electr. Veh. J.*, vol. 3, no. 1, pp. 875–883, 2009.
[19] A. Boglietti, A. Cavagnino, M. Lazzari, and M. Pastorelli, "Predicting iron losses in soft magnetic materials with arbitrary voltage supply: An engineering approach," *IEEE Trans. Magn.*, vol. 39, no. 2, pp. 981–989, Mar. 2003.
[20] L. Masisi, M. Ibrahim, J. Wanjiku, A. M. Aljehaimi, and P. Pillay, "The effect of two- and three-level inverters on the core loss of a synchronous reluctance machine (SynRM)," *IEEE Trans. Ind. Appl.*, vol. 52, no. 5, pp. 3805–3813, Sep. 2016.
[21] F. Preisach, "Über die magnetische Nachwirkung," *Zeitschrift für Phys. A Hadron. Nucl.*, vol. 94, no. 5–6, pp. 277–302, 1935.
[22] L. R. Dupre, R. Van Keer, and J. A. A. Melkebeek, "An iron loss model for electrical machines using the Preisach theory," *IEEE Trans. Magn.*, vol. 33, no. 5, pp. 4158–4160, Sep. 1997.
[23] A. Benabou, S. Clénet, and F. Piriou, "Comparison of Preisach and Jiles-Atherton models to take into account hysteresis phenomenon for finite element analysis," *J. Magn. Magn. Mater.*, vol. 261, no. 1–2, pp. 139–160, 2003.
[24] T. Chevalier, A. Kedous-Lebouc, B. Cornut, and C. Cester, "A new dynamic hysteresis model for electrical steel sheet," *Phys. B Condens. Matter*, vol. 275, no. 1–3, pp. 197–201, 2000.
[25] S. E. Zirka, Y. I. Moroz, P. Marketos, and A. J. Moses, "Viscosity-based magnetodynamic model of soft magnetic materials," *IEEE Trans. Magn.*, vol. 42, no. 9, pp. 2121–2132, Sep. 2006.
[26] A. Bergqvist, "Magnetic vector hysteresis model with dry friction-like pinning," *Phys. B Condens. Matter*, vol. 233, no. 4, pp. 342–347, Jun. 1997.
[27] C. X. C. Xiao, G. C. G. Chen, and W. G. H. Odendaal, "Overview of power loss measurement techniques in power electronics systems," *IEEE Trans. Ind. Appl.*, vol. 43, no. 3, pp. 657–664, May–Jun. 2007.
[28] M. Mu, F. C. Lee, Q. Li, D. Gilham, and K. D. T. Ngo, "A high frequency core loss measurement method for arbitrary excitations," in *Proc. 2011 26th Annu. IEEE Appl. Power Electron. Conf. Expo.*, 2011, pp. 157–162.

[29] J. Mühlethaler *et al.*, "Core losses under the DC bias condition based on Steinmetz parameters," *IEEE Trans. Power Electron.*, vol. 27, no. 2, pp. 953–963, Feb. 2012.
[30] V. J. Thottuvelil, T.G. Wilson, and H.A. Owen, Jr., "High-frequency measurement techniques for magnetic cores," *IEEE Trans. Power Electron.*, vol. 5, no. 1, pp. 41–53, Jan. 1990.
[31] J. K. Tangudu, T. M. Jahns, and A. EL-Refaie, "Core loss prediction using magnetic circuit model for fractional-slot concentrated-winding interior permanent magnet machines," in *Proc. 2010 IEEE Energy Convers. Congress Expo.*, 2010, pp. 1004–1011.
[32] M. Fratila, R. Ramarotafika, A. Benabou, S. Clénet, and A. Tounzi, "Stochastic post-processing calculation of iron losses—Application to a PMSM," *COMPEL-Int. J. Comput. Math. Electr. Electron. Eng.*, vol. 32, no. 4, pp. 1383–1392, Jul. 2013.
[33] N. Stranges and R. D. Findlay, "Measurement of rotational iron losses in electrical sheet," *IEEE Trans. Magn.*, vol. 36, no. 5 I, pp. 3457–3459, Sep. 2000.
[34] Y. Liu, S. K. Kashif, and A. M. Sohail, "Engineering considerations on additional iron losses due to rotational fields and sheet cutting," in *Proc. 2008 Int. Conf. Electr. Mach.*, 2008, pp. 1–4.
[35] M. Ranlof *et al.*, "Core loss prediction in large hydropower generators: Influence of rotational fields," *IEEE Trans. Magn.*, vol. 45, no. 8, pp. 3200–3206, Aug. 2009.
[36] B. Tekgun, A. R. Boynuegri, M. A. M. Chowdhury, and Y. Sozer, "Design and implementation of a sinusoidal flux controller for core loss measurements," in *Proc. 2016 IEEE Appl. Power Electron. Conf. Expo.*, 2016, pp. 207–214.
[37] A. J. Moses, N. Derebasi, G. Loisos, and A. Schoppa, "Aspects of the cut-edge effect stress on the power loss and flux density distribution in electrical steel sheets," *J. Magn. Magn. Mater.*, vol. 215, pp. 690–692, 2000.
[38] H. Ahlers and J. Ludke, "The uncertainties of magnetic properties measurements of electrical sheet steel," *J. Magn. Magn. Mater.*, vol. 215–216, pp. 711–713, 2000.
[39] N. Takahashi, H. Morimoto, Y. Yunoki, and D. Miyagi, "Effect of shrink fitting and cutting on iron loss of permanent magnet motor," *J. Magn. Magn. Mater.*, vol. 320, no. 20, pp. 925–928, 2008.
[40] F. Henrotte, J. Schneider, and K. Hameyer, "Influence of the manufacturing process in the magnetic properties of iron cores in induction machines," in *Proc. 2nd Int. Workshop Magn. Metallurgy*, 2006, pp. 352–360.
[41] R. Schifer and T. A. Lipo, "Core loss in buried magnet permanent magnet synchronous motors," *IEEE Trans. Energy Convers.*, vol. 4, no. 2, pp. 279–284, Jun. 1989.
[42] B. Tekgun, Y. Sozer, I. Tsukerman, P. Upadhyay, and S. Englebretson, "Core loss estimation in electric machines with flux controlled core loss tester," in *Proc. 2016 IEEE Energy Convers. Congress Expo.*, Milwaukee, WI, USA, pp. 1–7, doi: 10.1109/ECCE.2016.7854975.
[43] *Trial-Use Guide for Testing Permanent Magnet Machines*, *IEEE Std 1812-2014,* 2014.

**Burak Tekgun** (S'13–M'17) received the B.S. and M.Sc. degrees in electrical–electronics engineering from Cumhuriyet University, Sivas, Turkey, in 2008 and 2012, and the Ph.D. degree in electrical engineering from The University of Akron, Akron, OH, USA, in 2016.

His doctoral studies focused on high-frequency power electronics, core loss estimation of electric machines, and electric machine design and controls. He is currently an Assistant Professor in the Department of Electrical Electronics Engineering, Abdullah Gul University, Kayseri, Turkey. Prior to joining Abdullah Gul University, he was a Senior Research Engineer at AC Propulsion Inc., San Dimas, CA, USA. His current research interests include the areas of electric machines design and control, high-power, high-frequency power converters, wide-band-gap devices, core loss measurements, and modeling.

**Yilmaz Sozer** (M'05–SM'14) received the B.S. degree in electrical engineering from Middle East Technical University, Ankara, Turkey, in 1993, and the M.S. and Ph.D. degrees in electric power engineering from Rensselaer Polytechnic Institute, Troy, NY, USA, in 1995 and 2000, respectively.

His masters and doctoral work focused on power electronics and the development of control algorithms for electric machines. He is currently a Professor of the Department of Electrical and Computer Engineering, University of Akron, Akron, OH, USA, where is currently engaged in teaching and research. Before joining the university, he was with Advanced Energy Conversion Schenectady, NY, USA. His current research interests include in the areas of control and modeling of electrical drives, alternative energy systems, design of electric machines, high-power isolated dc/dc converter systems, static power conversion systems that interface energy storage, and distributed generation sources with the electric utility.

Dr. Sozer has been involved in IEEE activities that support power electronics, electric machines, and alternative energy systems. He is an Associate Editor and Paper Review Chair for the IEEE TRANSACTIONS ON INDUSTRY APPLICATIONS and the Associate Editor for the IEEE TRANSACTIONS ON POWER ELECTRONICS and the IEEE TRANSACTIONS ON TRANSPORTATION ELECTRIFICATION. He is a Chair for the IEEE IAS Renewable and Sustainable Energy Conversion Systems Committee.

**Igor Tsukerman** received the combined B.Sc./M.Sc. degree (with honors) in control systems in 1982 and the Ph.D. degree in electrical engineering from St. Petersburg Polytechnic, Saint Petersburg, Russia, in 1982 and 1988, respectively.

He is currently a Professor of Electrical and Computer Engineering at the University of Akron, Akron, OH, USA, where he has been a Faculty Member since 1995. His current research interests include applied electromagnetics, photonics, metamaterials, and homogenization theory. Tsukerman has over 200 refereed publications. He has authored the monograph *Computational Methods for Nanoscale Applications: Particles, Plasmons and Waves* (Springer 2008) and co-edited another book, *Plasmonics and Plasmonic Metamaterials* (World Scientific 2011). Currently, he is acting as the Editor-in-Chief of a five-volume reference set on electromagnetic analysis and simulation, to be published by World Scientific. Before coming to the University of Akron, he worked in the Department of Electrical and Computer Engineering, the University of Toronto (1990–1995).

**Parag Upadhyay** (M'03–SM'14) received the B.E. degree from Saurastra University, Gujarat, India, in 1992, and the M.Tech. and the Ph.D. degrees from the Indian Institute of Technology Delhi, New Delhi, India, in 2000 and 2006, all in electrical engineering.

During 1996 to 2008, he was a Faculty Member at Nirma University, Gujarat, and from 2008 to 2010, he was a Post-doctoral Fellow at the University of Minnesota. From 2010 to 2011, he was involved in teaching Electric Machines and Drives at SUNY Maritime College, New York City, NY, USA, as an Assistant Professor. Since 2011, he has been with ABB US Corporate research Center, Raleigh, NC, USA, as a Principal Research Scientist. He has led several technology development projects within ABB global research team in the area of electric machines, transformers, and electromagnetics. His current research interests include motor and transformer designs, electromagnetic parameter and performance estimations of electric machines, transformers, and electromagnetic devices.

**Steven Englebretson** received the Ph.D. degree in electrical engineering from the Massachusetts Institute of Technology, Cambridge, MA, USA, in 2009, and the B.Sc. degree in engineering from the Colorado School of Mines, Golden, CO, USA, in 2002.

Since 2013, he has been a Group Manager of the Electromagnetic Machines Group at the ABB Corporate Research Center, Raleigh, NC, USA. He joined ABB in 2009 as a Research Scientist at the US Corporate Research Center on the design and analysis of electric machines and has been involved with several R&D projects progressing ABB frontiers on energy efficiency, cost minimization, and renewable energy applications.